# A Radio-Frequency Tunable Active Filter

ALLEN TAFLOVE AND MORRIS E. BRODWIN

*Abstract*—**A design approach for a tunable active filter of constant bandwidth and center-frequency gain is described. The approach is based on a feedback configuration with a complex pole pair in the forward transfer function, and a complex zero pair in the feedback transfer function. Center frequency tuning is achieved with the variation of only one element, a potentiomenter, which controls the feedback loop gain. A circuit realization using two commercial video amplifiers with RC embedding is presented. A tuning range of 25 percent at 5 MHz, with a nominal bandwidth of 90 kHz or 180 kHz, and a variation of center-frequency gain of less than ±1 dB over the tuning range, is obtained.**

## I. Introduction

A demanding problem in active network synthesis is the design of a frequency-selective amplifier (FSA) with the following characteristics: 1) moderate $Q$, tunable center frequency operation above 1 MHz; 2) center frequency tunable with only one element; 3) constant bandwidth and center-frequency gain over the tuning range; 4) low sensitivity of center frequency and $Q$ to variations in the gains of active elements. The circuit described below meets these specifications, using low cost commercial differential video amplifiers, and is usable up to at least 10 MHz.

## II. Theory

The ideal tunable FSA pole locus is seen in Fig. 1(a). Boxes mark the position of the complex-conjugate FSA pole pair with respect to some tuning parameter. The real part of the pole pair remains constant as its frequency is varied from zero to infinity. A filter realizing such a pole locus, in addition to a simple zero at the origin, possesses a constant bandwidth over an infinite tuning range.

The pole locus if Fig. 1(b) represents an approximation of the ideal locus of Fig. 1(a) over a selected frequency range. This approximation is realized by the circuit discussed in this paper as a feedback system root locus. The feedback system, depicted schematically in Fig. 2, has a complex pole pair in $H_1(s)$, the forward transfer function, and a complex zero pair in $H_2(s)$, the feedback transfer function. Upon closing the feedback loop, the system generates the overall FSA transfer function $H(s)$

$$H(s) = \frac{V_{out}}{V_{in}}(s) = \frac{H_1(s)H_3(s)}{1 + B_0H_1(s)H_2(s)}. \tag{1}$$

The pair of locus branches of $H(s)$ originate at the complex pole pair of $H_{1b}(s)$ and terminate at the complex zero pair of $H_2(s)$. The position of a pole of $H(s)$ on each locus branch is set by the loop gain control $B_0$. By positioning the pole locus end points along a vertical line in the $s$-plane, only the frequency of the pole pair of $H(s)$ changes as $B_0$ is varied. The maximum FSA tuning range is determined by the frequency difference between the pole locus end points.

In Fig. 2, $H_{1b}(s)$ is the transfer function of a fixed-frequency, active RC FSA. We choose $H_{1b}(s)$ to be realized by the negative real axis phantom zero FSA discussed by Kerwin [1]. This choice is motivated by the fact that Kerwin's FSA achieves a small $Q$-sensitivity with respect to the gains of

Manuscript received February 26, 1973; revised October 15, 1973.
The authors are with the Department of Electrical Engineering, Technological Institute, Northwestern University, Evanston, Ill. 60201.

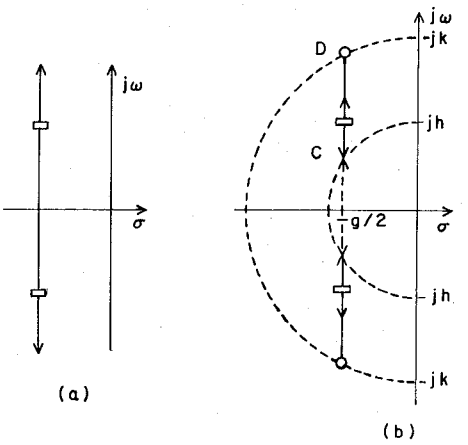


Fig. 1. Pole loci considered for variable frequency FSA's.

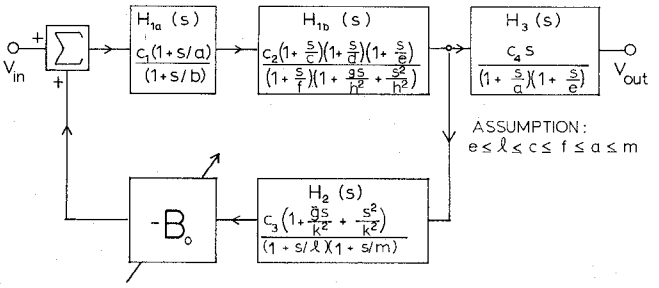


Fig. 2. Block diagram of a constant-bandwidth tunable FSA.

active elements. The result of this choice is the generation of a third-order transfer function for $H_{1b}(s)$, with three real zeroes, one real pole, and the conjugate pole pair. To compensate the effects of the real singularities of $H_{1b}(s)$, a lag-lead passive RC network realizing $H_{1a}(s)$ is required. We choose $H_2(s)$ to be realized by a RC twin-T network, which generates two real poles as a byproduct of the desired conjugate zero pair.

To approximate $H(s)$, we choose the real singularities of $H_{1a}(s)$ and $H_2(s)$ to satisfy the following approximations:

$$a \approx m, \qquad b \approx d, \qquad l \approx e. \tag{2}$$

For simplicity, let us further assume

$$c \approx f, \qquad g \approx \tilde{g}, \qquad \overline{B_0} = B_0c_1c_2c_3. \tag{3}$$

Then, we may approximate $H(s)$ as

$$H(s) \approx \frac{c_1c_2c_4s}{(1 + gs/h^2 + s^2/h^2) + \overline{B_0}(1 + gs/k^2 + s^2/k^2)}. \tag{4}$$

The pole locus of $H(s)$ of (4) is plotted in Fig. 1(b). Defining the FSA center frequency as

$$\omega_p = \left[\frac{k^2(1 + \overline{B_0})}{(k/h)^2 + \overline{B_0}}\right]^{1/2}$$

and the quantity $A_0 = [c_1c_2c_4k^2]/[(k/h)^2 + \overline{B_0}]$, we may rewrite (4) as

$$H(s) \approx \frac{A_0s}{s^2 + gs + \omega_p^2}. \tag{5}$$

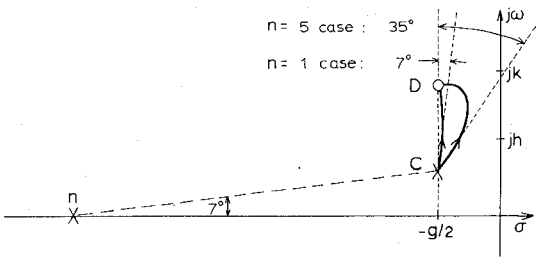


Fig. 3. Examples of nonideal constant-bandwidth pole loci.

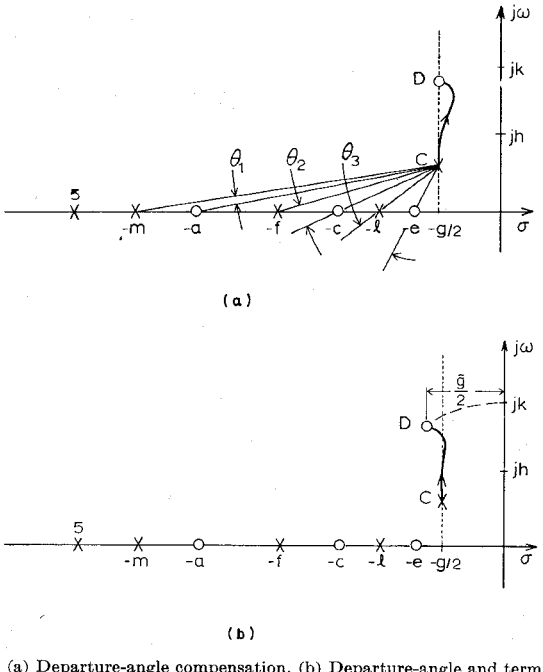


Fig. 4. (a) Departure-angle compensation. (b) Departure-angle and termination-damping compensation.

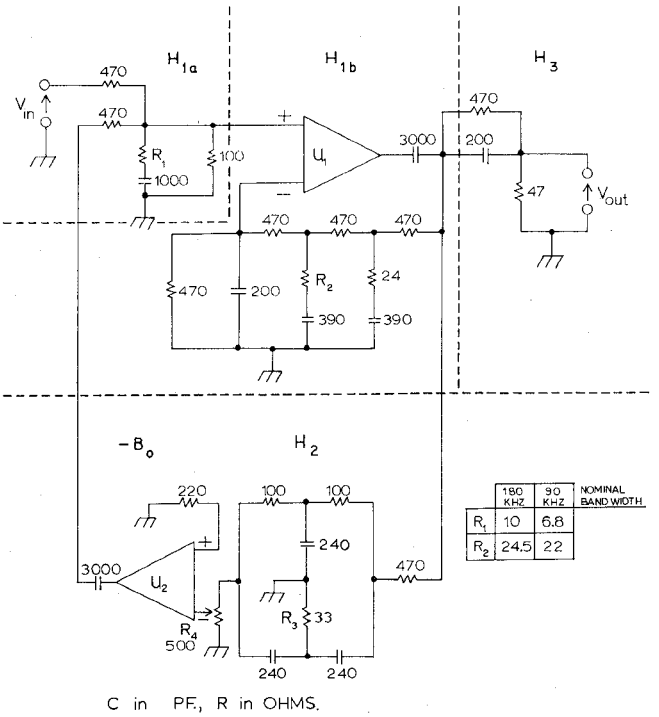


Fig. 5. Realization of the 5-MHz tunable FSA.

$H(s)$ has a magnitude characteristic that peaks at $\omega_p$, a 3 dB bandwidth equal to $g$, and a peak value of $A_0/g$. The bandwidth remains constant as the center frequency is increased by increasing $B_0$. However, the peak value declines as $B_0$ increases. This decrease can be approximately cancelled by modifying $H_3(s)$ to introduce a frequency emphasis factor.

The next problem to be considered is the effect of excess open-loop phase lag introduced by the use of finite bandwidth gain blocks. To simulate this condition, we add $n$ negative-real-axis poles to the open-loop transfer function of the feedback system of Fig. 2. The resulting pole locus plots, for the cases $n = 1$ and $n = 5$, are seen in Fig. 3. The locus branches from the multiple real pole and those in the lower-half plane are omitted for the sake of clarity. We see that excess phase lag bulges the pole locus to the right. If the locus origin at $C$ is of moderate $Q$, this bulging effect could lead to the locus crossing into the right-half plane, and thus, to FSA instability.

The bulging distortion can be efficiently reduced by proper selection of two locus parameters: departure angle from the locus origin at $C$, and damping of the locus termination at $D$. The degree of each of these types of compensation can be controlled by adjustment of the zeros of $H_{1a}(s)$ and $H_2(s)$, as will now be shown.

To achieve departure angle compensation, we modify the assumptions of (2) and (3) by letting $a < m$, $c < f$, $e < l$. This modification is equivalent to adding three lead-lag networks to the basic open-loop transfer function. The modified pole locus is seen in Fig. 4(a). The equivalent lead-lag networks rotate the departure angle vector at $C$ counterclockwise by an angle equal to $\theta_1 + \theta_2 + \theta_3$. $\theta_2$ and $\theta_3$ are fixed upon selection of $H_{1b}(s)$ and $H_2(s)$. However, $\theta_1$ can be adjusted independently of the others by shifting the zero of $H_{1a}(s)$ along the real axis. With proper adjustment of the position of this zero, the departure angle is made 90°, so that the pole locus is initially parallel to the frequency axis.

To adjust the damping of the locus termination, we assume that $g < \tilde{g}$. This causes the zero at $D$ to be further from the frequency axis than the pole at $C$. The modified pole locus is seen in Fig. 4(b). The locus termination damping is experimentally selected to shift locus bulging to the left so that the best possible straight vertical line is obtained. This adjustment may be made independently of the other locus parameters.

There exists nearly optimum combinations of the two types of pole locus compensation discussed. In practice, this technique allows a tunable pole locus, meeting specifications for bandwidth and peak gain variation, to be established. The technique should work well for narrow bandwidth operation at low frequencies, where the effects of band-limited amplifiers are minimal, and for moderate bandwidth operation at radio frequencies.

## III. Experimental Realization

The experimental realization was selected to operate at about 5 MHz to illustrate the compensation capabilities of the circuit. For operation at lower frequencies, we need only scale the value of each capacitor used in the realization, and reduce the amount of compensation.

The schematic diagram of the circuit realization is seen in Fig. 5, which is partitioned to indicate the realization of each transfer function block of Fig. 2. Component values for a 180-kHz and a 90-kHz bandwidth FSA, tunable over the range 4.7–5.9 MHz, are given. $U_1$ and $U_2$ are two SN72733 differential video amplifiers, commercial integrated circuits in 14 pin dual-in-line packages. $U_1$ operates in its maximum voltage gain of 150 mode, while $U_2$ operates in the minimum gain of 5 mode. $U_1$ has a gain characteristic that can be approximated by a pole pair at about −50 MHz near the real axis,

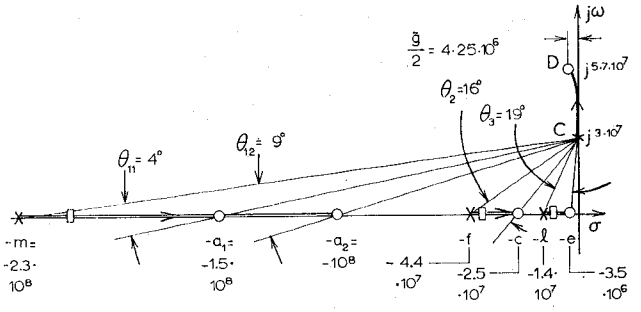


Fig. 6. Pole locus diagram of the 5-MHz tunable FSA.

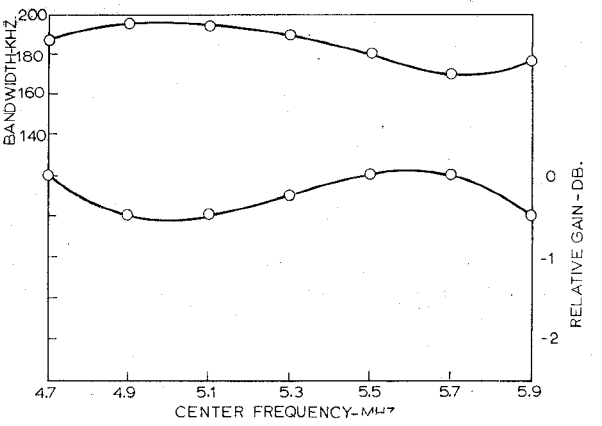


Fig. 7. Bandwidth and gain at center frequency as a function of the center frequency of the 180-kHz bandwidth tunable FSA.

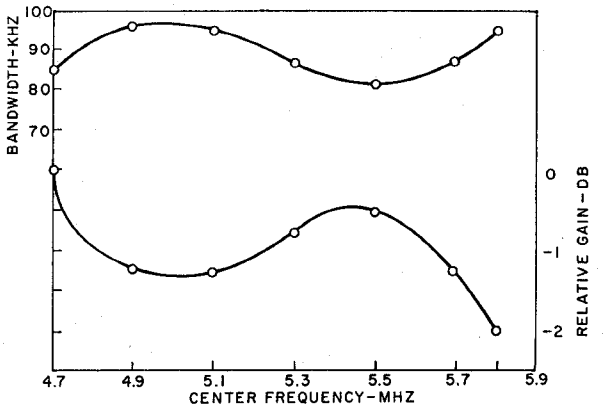


Fig. 8. Bandwidth and gain at center frequency as a function of the center frequency of the 90-kHz bandwidth tunable FSA.

while $U_2$ can be characterized by a damped conjugate pole pair at about $-100$ MHz. The excess phase lag introduced by $U_1$ and $U_2$ is sufficient to require the application of the pole locus compensation methods of Fig. 4. The resulting FSA pole locus is seen in Fig. 6. The total required counterclockwise rotation of the departure angle vector at $C$ is 44° for the 180-kHz bandwidth FSA, and 39° for the 90-kHz bandwidth FSA. It was found necessary to increase the damping of the locus termination at $D$ to a level much greater than that at $C$ in order to achieve the maximum tuning range. This increased locus termination damping, however, prevents constant-bandwidth tuning above 5.9 MHz, where the locus curves sharply to the left. It was not found necessary to change the locus termination damping for each nominal bandwidth FSA.

Adjustment of $R_1$ from 7 Ω to 10 Ω changes $\theta_1$ from 4°, suitable for a 90-kHz bandwidth, to 9°, suitable for a 180-kHz bandwidth FSA. $R_1$ fixes the position of the zero of $H_{1a}(s)$, and thus, the coefficient $a$. $R_2$ fixes the nominal bandwidth of the tunable FSA by adjusting the real part of the locus origination points, the pole pair of $H_{1b}(s)$. The system bandwidth is seen to be a sensitive function of the value of $R_2$. $R_3$ controls the damping of the locus termination points, and was left fixed for both cases. $R_4$ is a potentiometer that controls the loop gain, and thus, the frequency of FSA operation, by setting $B_0$. Because the inverting terminal of $U_2$ presents high impedance to $R_4$, this frequency adjustment may be made independently of the other circuit parameters. Once the system bandwidth is fixed by $R_2$, and the compensation fixed by $R_1$ and $R_3$, we need only vary $R_4$ to tune the FSA.

All passive components used in the circuit realization were discrete. The circuit was constructed on a standard double-sided glass epoxy circuit board, with one side used as a ground plane. $R_4$ was a board-mounted cermet trimmer with small parasitic inductance and capacitance.

## IV. Experimental Results

Figs. 7 and 8 represent the experimental results for the 180-kHz and the 90-kHz bandwidth tunable filters. The bandwidth and the relative center-frequency gain of each tunable filter is plotted versus center frequency. Deviations from the nominal may be interpreted as a failure of the experimental pole locus to exactly parallel the frequency axis in the $s$-plane.

The 180-kHz bandwidth tunable filter has a bandwidth spread of about ±8 percent about nominal, and a center-frequency gain spread of about $\pm\frac{1}{4}$ dB, over the tuning range of 4.7 MHz to 5.9 MHz. The 90-kHz bandwidth tunable filter has a bandwidth spread of ±9 percent about nominal, with a gain spread of ±1 dB, over the same tuning range. The tuning range, about 1.2 MHz (25 percent), may be increased by adding gain to the feedback transfer function $H_2(s)$ with $U_2$, but at the cost of decreased bandwidth and center-frequency gain constancy over the whole tuning range. We see that meeting specifications for bandwidth and gain constancy becomes more difficult as the nominal bandwidth is reduced. However, bandwidths of somewhat less than 90 kHz can be used here with perfect stability. For the same FSA circuit operating at a lower frequency, where the effect of excess amplifier phase lag is reduced, higher $Q$ loci should

be attainable with comparable limits on center-frequency gain and bandwidth variation over the tuning range.

## V. Conclusions

The FSA described in this correspondence is suitable for tunable center-frequency, constant bandwidth, and constant center-frequency voltage gain operation over a sigificant tuning range above 1 MHz. The frequency of the tunable FSA is varied by only one element, a potentiometer. Compensation for best tuning characteristics is accomplished with the selection of three fixed resistors, controlling bandwidth, pole locus departure angle, and pole locus termination damping. With the circuit described, stable tunable operation is possible over a 25 percent tuning range at 5 MHz for bandwidths of 90 kHz.

## References

[1] W. J. Kerwin, "Active R-C network synthesis using voltage amplifiers," in *Active Filters: Lumped, Distributed, Digital, and Parametric*, L. P. Huelsman, Ed. New York: McGraw-Hill, 1970, pp. 44-47.

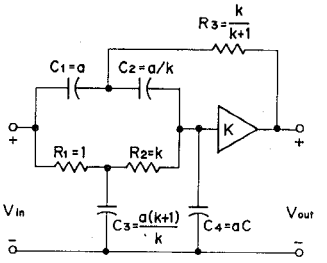


Fig. 1. Twin-tee $J$ axis zero network.

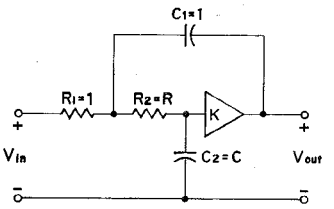


Fig. 2. Low-pass section.

# Design of a Hybrid Integrated Circuit Elliptic Active *RC* Filter

GERALD T. VOLPE AND LEROY M. FREEMAN

***Abstract*—This paper discusses design details and experimental results obtained in realizing hybrid IC sharp rolloff filters. Practical low and high pass audio active *RC* filters were produced in large quantities with rolloff characteristics of approximately 500 dB/octave.**

## I. Introduction

At present, the need for very small, low cost filters with sharp frequency cutoff characteristics is compatible with hybrid integrated circuit technology. This correspondence discusses the design and implementation of a class of active *RC* Cauer filters whose coefficients are computed from Jacobian elliptic functions.

The circuits of Figs. 1 and 2 first suggested by Sallen and Key [2] realize the class of Elliptic filters. The circuit of Fig. 1 contains a twin-tee *RC* circuit which realizes required $j$ axis transmission zeros. It is these transmission zeroes placed close to the band edge that give rise to the high rate of rolloff. The low-pass filter section of Fig. 2 is required since the overall filter must eventually rolloff at high frequencies. These circuits were selected because a minimum number of passive components and operational amplifiers are required compared to other techniques such as state variable filters or gyrator configurations [3]. This implies a power and cost savings making the implementation of such a filter on a hybrid IC chip feasible.

The implementation of a hybrid IC filter also leads to several interesting problems. The main problem is that the high rate of rolloff implies a high $Q$ on at least one stage, which implies high sensitivity on that stage. Consequently, tight tolerances and low temperature coefficients are needed.

Another unique problem in a hybrid IC is that trimming must be kept minimal and unidirectional. In addition, available component sizes impose limitations on the spread of component values.

Another important problem encountered was the choice of operational amplifiers, since the synthesis technique that is suggested in the literature [2] does not account for gain and phase variations in the $K$ amplifier. In this work, it was found that even small variations in gain magnitude and phase can imply appreciable errors in the filter's response. Since these variations originate from the open loop response of the op-amp, the choice of amplifier and method of compensation was studied. The result was that the two-pole compensation scheme was required for the LM101 in the two highest $Q$ stages, while, internally compensated 741 op-amp sufficed for the remainder of the lower $Q$ stages.

## II. Theoretical Model-Ideal Filter by Synthesis

A synthesis procedure was performed for a low-pass filter which motivated this work. The specifications are that it have unity gain with $\pm 0.25$-dB ripple up to a corner frequency of 4600 Hz, and that it be $-55$ dB down at 5200 Hz. These specifications suggest an eighth order elliptic filter [1]. Consulting filter tables [1] leads to the explicit transfer function,

$$\frac{V_0}{V_s}(p) = \frac{0.4(1.0363)[1 + 0.3490p^2][1 + 0.7672p^2][1 + 0.6420p^2]}{1.0363 + 4.3653p + 11.708p^2 + 19.7021p^3 + 29.2059p^4 + 26.5881p^5 + 26.1384p^6 + 11.1952p^7 + 7.6073p^8} \tag{1}$$

or equivalently

$$\frac{V_0}{V_s}(p) = \frac{0.4(0.0234)[p^2 + 2.8654][p^2 + 1.3039][p^2 + 1.5577]}{[p^2 + 0.1903p + 0.903][p^2 + 0.7743p + 0.2418][p^2 + 0.459p + 0.6104]\cdot[p^2 + 0.0481p + 1.02233]}. \tag{2}$$

Manuscript received June 8, 1973; revised November 5, 1973.

G. T. Volpe is with the Department of Electrical Engineering, Cooper Union School of Engineering and Science, New York, N. Y.
L. M. Freeman is with the Department of Hybrid Integrated Circuits, General Instrument Corporation, Hicksville, N. Y.

On the basis of the realization being performed by cascaded buffer sections one can identify the stage transfer functions as